Front. Optoelectron. China 2010, 3(3): 270–282
DOI 10.1007/s12200-010-0106-9

RESEARCH ARTICLE

Theoretical demonstration for signal gain in multiple four-wave mixing processes based on cubic susceptibility medium

Liang ZHAO, Junqiang SUN (✉), Zhefeng HU, Qian HU, Yujie ZHOU, Jing SHAO, Tianye HUANG, Jun LI

Wuhan National Laboratory for Optoelectronics, College of Optoelectronic Science and Engineering, Huazhong University of Science and Technology, Wuhan 430074, China

© Higher Education Press and Springer-Verlag Berlin Heidelberg 2010

Abstract An insight into the signal gain in multiple four-wave mixing (MFWM) processes based on a cubic susceptibility medium is theoretically proposed and demonstrated. A dual-pumped fiber optical parametric amplification (FOPA) model is developed with the exact expressions for the signal gain and its 3-dB bandwidth successfully yielded. With these analytical expressions, we show that when pump-1 and pump-2 wavelengths tuned at 1549 and 1551.02 nm, the 3-dB bandwidth of the signal gain can be achieved at about 2253.4 nm theoretically by properly setting the pumped powers. Numerical simulations show that there is a small pinnacle emerging in the signal gain spectrum owing to the degenerate OPA process occurring. The proposed OPA model can find potential applications in all-optical wavelength conversion, optical amplifier, and all-optical sampling.

Keywords fiber optical parametric amplification (FOPA), four-wave mixing, highly nonlinear fiber, signal gain spectrum, 3-dB bandwidth

1 Introduction

Recently, fiber optical parametric amplifications (FOPAs) can find potential applications in optical wavelength converter [1,2], optical amplifiers [1], dispersion monitoring [3], all-optical sampling [4], optical pulse generating [5], and notch filter [6]. In the conventional FOPA configuration, energy will generally be transferred from an intense pump wave with frequency ω_p to a weak signal wave with frequency ω_s and the generated sideband with frequency ω_i, owing to an optical parametric process and a multiple four-wave mixing (MFWM) process simultaneously occurring in the fiber. In the case of a continuous signal wave, either single-pump or dual-pumped FOPAs have been studied extensively in recent years. Hansryd, Andrekson, et al. [1] have theoretically and experimentally demonstrated that the maximum signal gain is approximately 60 dB, and its bandwidth is approximately 70 nm with a single pumping source, but the signal gain spectrum is not flat. Gao et al. [7] have proposed a new dual-pumped FOPA structure, which is composed of three-section photonic crystal fibers (PCFs) and theoretically provides a nearly flat gain of 21.54 dB with peak-to-peak gain uniformity of better than 0.2 dB over the 405-nm bandwidth from 1260 to 1665 nm. In 2005, Liu et al. [8] have theoretically proposed and experimentally demonstrated MFWM self-stability with only two pumps in optical fibers. In 2008, Liu et al. [9] further have developed the MFWM model with multi-frequency pumps and have experimentally confirmed their theory.

However, to our best knowledge, the conventional dual-pumped FOPA [7] model is considered that only the non-degenerated process takes place in the fiber, and this model is not exact in the realistic circumstance. In fact, both degenerate and non-degenerate parametric processes will occur in the dual-pumped FOPA. In this paper, the signal gain is analyzed under the un-depleted mode, and we have yielded an analytical expression for signal gain by simultaneously considering the degenerated and non-degenerated four-wave mixing (FWM) contributions. Calculation results indicate that there is a small pinnacle emerging in the signal gain spectrum which is different from the results of previous literatures [5,7]. In addition, the 3-dB bandwidth of the signal gain is also discussed, which can be attained ~2253.4 nm theoretically by properly setting the pumping powers and wavelengths.

Received April 6, 2010; accepted May 26, 2010

E-mail: jqsun@mail.hust.edu.cn

The theoretical results can be an effective theoretical basis for future experimental investigation of FOPA.

2 Working principle

In the dual-pumped FOPA model, the degenerate and non-degenerate FWM will compete with each other, leading to new sideband generation. Figure 1 presents the schematic diagram of frequency components when two pumps (ω_{p1} and ω_{p2}) with a weak signal (ω_s) launched into a highly non-linear fiber (HNLF). In an intuitive approach, the non-degenerated process starts with two pump waves that propagate together into the fiber. As they propagate, they will continuously beat with each other; the sidebands with frequencies $\omega_i = \omega_{p1} + (\omega_{p1} - \omega_{p2})$ and $\omega_{i'} = \omega_{p2} + (\omega_{p2} - \omega_{p1})$ are generated, consuming the pump wave powers, which is bad for signal wave amplification. When a third wave (ω_s, weak signal wave) is added, degenerated and non-degenerated FWM will simultaneously happen in HNLF. During the degenerate FWM (DFWM) process, two idlers (ω_{i1},ω_{i2}) will be generated when two continuous-wave (CW) optical waves (ω_{p1},ω_{p2}) are injected, satisfying the relationship of $2\omega_{p1} = \omega_s + \omega_{i1}$ and $2\omega_{p2} = \omega_s + \omega_{i2}$. During the non-degenerate FWM (NFWM) process, the idler (ω_{i12}) will be generated owing to the interaction of three launched waves (ω_s,ω_{p1},ω_{p2}), satisfying the relationship of $\omega_{i12} = \omega_{p1} + \omega_{p2} - \omega_s$, and all the relations among the injected waves and sidebands are shown in Fig. 1. The above-mentioned three processes are beneficial for signal wave amplification. In order to simplify the above-mentioned processes, we introduce the notion of "equivalent pump powers" to ignore the FWM happening between pumps. The notion of "equivalent pump powers" is based on the following hypotheses. Firstly, "equivalent pump powers" describe the pump powers that are only utilized to amplify the signal. Secondly, when suppressing the FWM between pumps through setting large linear phase mismatch [10], the pumping powers can almost be used to amplify the signal. Therefore, we can neglect the FWM happening between pumps by setting proper wavelengths or powers. Figure 2 illustrates the schematic diagram of the MFWM process ignoring DFWM happening between pumps, from which it can clearly be seen that the sidebands with frequency ω_i and $\omega_{i'}$ are no longer emerging in the spectrum.

3 Derivation of signal gain expression

When two intense pump waves (ω_{p1},ω_{p2}) and one signal wave (ω_s) are injected into the HNLF, the FWM process is most easily described if assuming collinearly polarized three intensive waves. In this case, the walk-off, absorption and dispersion terms in nonlinear Schrödinger equations (NLSs) are negligible compared to the nonlinear terms. When we consider the non-degenerate FWM case, NLS equations that describe the evolution of waves in the fiber are expressed as follows [6,11,12]:

$$\frac{dA_{p1}}{dz} = i\gamma[|A_{p1}|^2 + 2(|A_{p2}|^2 + |A_s|^2 + |A_{i12}|^2)]A_{p1} + 2i\gamma A_{p2}^* A_s A_{i12} \exp(i\Delta\beta_3 z), \quad (1)$$

$$\frac{dA_{p2}}{dz} = i\gamma[|A_{p2}|^2 + 2(|A_{p1}|^2 + |A_s|^2 + |A_{i12}|^2)]A_{p2} + 2i\gamma A_{p1}^* A_s A_{i12} \exp(i\Delta\beta_3 z), \quad (2)$$

$$\frac{dA_s}{dz} = i\gamma[|A_s|^2 + 2(|A_{p1}|^2 + |A_{p2}|^2 + |A_{i12}|^2)]A_s + 2i\gamma A_{i12}^* A_{p1} A_{p2} \exp(-i\Delta\beta_3 z), \quad (3)$$

$$\frac{dA_{i12}}{dz} = i\gamma[|A_{i12}|^2 + 2(|A_{p1}|^2 + |A_{p2}|^2 + |A_s|^2)]A_{i12} + 2i\gamma A_s^* A_{p1} A_{p2} \exp(-i\Delta\beta_3 z). \quad (4)$$

When we consider the degenerate FWM happening between the pump (ω_{p1}) and the signal (ω_s), NLS equations can be given by [6,11,12]

$$\frac{dA_{p1}}{dz} = i\gamma[|A_{p1}|^2 + 2(|A_s|^2 + |A_{i1}|^2)]A_{p1} + 2i\gamma A_{p1}^* A_s A_{i1} \exp(i\Delta\beta_1 z), \quad (5)$$

$$\frac{dA_s}{dz} = i\gamma[|A_s|^2 + 2(|A_{p1}|^2 + |A_{i1}|^2)]A_s + i\gamma A_{i1}^* A_{p1}^2 \exp(-i\Delta\beta_1 z), \quad (6)$$

$$\frac{dA_{i1}}{dz} = i\gamma[|A_{i1}|^2 + 2(|A_{p1}|^2 + |A_s|^2)]A_{i1}$$

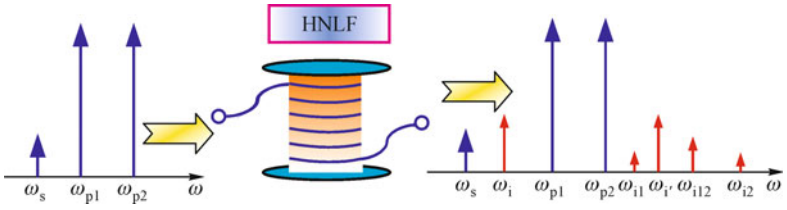


Fig. 1 Schematic diagram of frequency components when two pumps (ω_{p1} and ω_{p2}) with a weak signal (ω_s) launched into HNLF

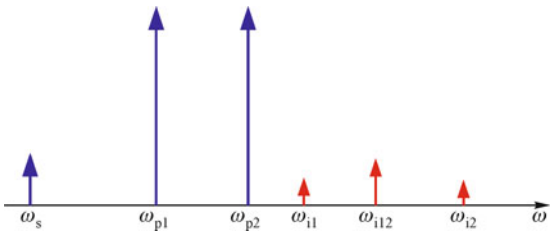


Fig. 2 Schematic diagram of MFWM process ignoring DFWM happening between pumps

$$+ i\gamma A_s^* A_{p1}^2 \exp(-i\Delta\beta_1 z). \quad (7)$$

When we consider the degenerate FWM happening between the pump (ω_{p2}) and the signal (ω_s), NLS equations can be written as follows [6,11,12]:

$$\frac{dA_{p2}}{dz} = i\gamma[|A_{p2}|^2 + 2(|A_s|^2 + |A_{i2}|^2)]A_{p2} + 2i\gamma A_{p2}^* A_s A_{i2} \exp(i\Delta\beta_2 z), \quad (8)$$

$$\frac{dA_s}{dz} = i\gamma[|A_s|^2 + 2(|A_{p2}|^2 + |A_{i2}|^2)]A_s + i\gamma A_{i2}^* A_{p2}^2 \exp(-i\Delta\beta_2 z), \quad (9)$$

$$\frac{dA_{i2}}{dz} = i\gamma[|A_{i2}|^2 + 2(|A_{p2}|^2 + |A_s|^2)]A_{i2} + i\gamma A_s^* A_{p2}^2 \exp(-i\Delta\beta_2 z), \quad (10)$$

where $\Delta\beta_j$ ($j = 1,2,3$) is the linear phase mismatch term. In the realistic circumstance, the three FWM processes happen at the same time in HNLF. By investigating, it is found that we can assume the three processes happen in any sequence when calculating the signal gain in the non-depletion mode, i.e., the two degenerate FWMs happen firstly, and then the non-degenerate FWM happens. With the assumption, the approximate analytic signal gain solution of Eqs. (5)–(7) can be given by [1]

$$G_{s1} = 10\log\left[1 + \left(\frac{\gamma P_{p1}}{g_1}\sinh(g_1 L)\right)^2\right], \quad (11)$$

where L is the fiber length, γ is the nonlinear coefficient, and g_1 stands for the parametric gain coefficient which is determined by [1]

$$\begin{aligned} g_1^2 &= [(\gamma P_{p1})^2 - (\kappa_1/2)^2] = -\Delta\beta_1\left(\frac{\Delta\beta_1}{4} + \gamma P_{p1}\right), \\ \Delta\beta_1 &= -\frac{2\pi c}{\lambda_0^2}\frac{dD}{d\lambda}(\lambda_{p1} - \lambda_0)(\lambda_{p1} - \lambda_s)^2, \\ \kappa_1 &= \Delta\beta_1 + 2\gamma P_{p1}, \end{aligned} \quad (12)$$

where $\Delta\beta_1$ is the linear phase mismatch term, κ_1 is the total phase mismatch term, λ_{p1} is the pump-1 wavelength, λ_0 is the zero dispersion wavelength, λ_s is the signal wavelength, $\frac{dD}{d\lambda}$ is the dispersion slope, and c is the light velocity in the vacuum. In order to yield the maximum value of G_{s1}, setting $G_{s1}' = 0$, we can obtain the results

$$g_1 = 0 \text{ or } \sinh(g_1 L)/(g_1 L) = 0. \quad (13)$$

In the same way, we can get the approximate solution of Eqs. (8)–(10) given by [1]

$$G_{s2} = 10\log\left[1 + \left(\frac{\gamma P_{p2}}{g_2}\sinh(g_2 L)\right)^2\right], \quad (14)$$

where

$$\begin{aligned} g_2^2 &= [(\gamma P_{p2})^2 - (\kappa_2/2)^2] = -\Delta\beta_2\left(\frac{\Delta\beta_2}{4} + \gamma P_{p2}\right), \\ \Delta\beta_2 &= -\frac{2\pi c}{\lambda_0^2}\frac{dD}{d\lambda}(\lambda_{p2} - \lambda_0)(\lambda_{p2} - \lambda_s)^2, \\ \kappa_2 &= \Delta\beta_2 + 2\gamma P_{p2}. \end{aligned} \quad (15)$$

In order to get the maximum value of G_{s2}, we should satisfy the condition given by

$$g_2 = 0 \text{ or } \sinh(g_2 L)/(g_2 L) = 0. \quad (16)$$

We can get the signal gain by solving Eqs. (1)–(4) [1], as

$$G_{s12} = 10\log\left[1 + \left(\frac{\mu r}{g_{12}}\sinh(g_{12} L)\right)^2\right], \quad (17)$$

where

$$\begin{aligned} \mu &= \gamma(P_{p1} + P_{p2}), \\ r &= 2\sqrt{P_{p1}P_{p2}}/\sqrt{P_{p1}^2 + P_{p2}^2}, \\ g_{12}^2 &= (\mu r)^2 - (\kappa_{12}/2)^2, \\ \kappa_{12} &= \Delta\beta_{12} + \mu, \\ m &= \pi\lambda_0^3 c\frac{dD}{d\lambda}\left[\lambda_0\left(\frac{1}{\lambda_{p1}} + \frac{1}{\lambda_{p2}}\right) - 2\right], \\ \Delta\beta_{12} &= m\left(\frac{1}{\lambda_s} - \frac{1}{\lambda_{p1}}\right)\left(\frac{1}{\lambda_s} - \frac{1}{\lambda_{p2}}\right). \end{aligned} \quad (18)$$

In order to get the maximum value of G_{s12}, we should satisfy the condition given by

$$g_{12} = 0 \text{ or } \sinh(g_{12} L)/(g_{12} L) = 0. \quad (19)$$

Therefore, the total signal gain can be written as

$$G_s = G_{s1} + G_{s2} + G_{s12}. \quad (20)$$

Once the first equations of Eqs. (13), (16) and (19) are simultaneously satisfied, the signal gain will achieve its maximum value, whereas when the second equations of them are met, the side lobe valley of the signal gain is zero.

Based on the above analysis, a maximum signal gain can be attained if the subsequent equations satisfied

$$\begin{cases} g_1 = 0, \\ g_2 = 0, \\ g_{12} = 0. \end{cases} \tag{21}$$

And thus, the maximum value of the signal gain is given by

$$G_{\mathrm{s}} = 10\log\left[\left(1+(\gamma P_{\mathrm{p1}}L)^2\right)\left(1+(\gamma P_{\mathrm{p2}}L)^2\right) \cdot\left(1+(\mu rL)^2\right)\right]. \tag{22}$$

As for Eq. (21), we should note that a fine phase matching condition cannot be obtained in reality to simultaneously satisfy Eq. (21). Hence, the actual maximum value of the signal gain is difficult to attain the value expressed by Eq. (22). But Eq. (22) gives us the hints for increasing the signal gain: a) increase the nonlinear coefficient; b) increase the fiber length; c) increase the launched pumping power. However, the bad effects of the above performances are mainly embodied from the following three aspects. Firstly, the nonlinear coefficient is variable with the injected wave frequency, but not very distinct, so Eq. (22) is not accurate. Secondly, as the signal wave power periodically varies with the fiber length, increasing the fiber length is available to transfer the energy from the signal wave back to the pump wave, so the signal gain may decrease when the fiber length is too long. Finally, when increasing the launched pumping power, it may generate other bad nonlinear effects, i.e., the stimulated Brillouin scatter effect. So we should synthetically take account of the above methods to increase the signal gain. Furthermore, the solutions of Eq. (21) can be given by

$$\begin{cases} \lambda_{\mathrm{s}} = \lambda_{\mathrm{p1}},\ \lambda_{\mathrm{s}} = \lambda_{\mathrm{p1}} \pm \lambda_0\sqrt{\dfrac{2\gamma P_{\mathrm{p1}}}{\pi c\dfrac{\mathrm{d}D}{\mathrm{d}\lambda}(\lambda_{\mathrm{p1}}-\lambda_0)}}, \\ \lambda_{\mathrm{s}} = \lambda_{\mathrm{p2}},\ \lambda_{\mathrm{s}} = \lambda_{\mathrm{p2}} \pm \lambda_0\sqrt{\dfrac{2\gamma P_{\mathrm{p2}}}{\pi c\dfrac{\mathrm{d}D}{\mathrm{d}\lambda}(\lambda_{\mathrm{p2}}-\lambda_0)}}, \\ \lambda_{\mathrm{s}} = \dfrac{2}{\dfrac{1}{\lambda_{\mathrm{p1}}}+\dfrac{1}{\lambda_{\mathrm{p2}}} \pm \sqrt{\left(\dfrac{1}{\lambda_{\mathrm{p1}}}-\dfrac{1}{\lambda_{\mathrm{p2}}}\right)^2+\dfrac{4\mu(2r-1)}{m}}} \\ \text{or } \lambda_{\mathrm{s}} = \dfrac{2}{\dfrac{1}{\lambda_{\mathrm{p1}}}+\dfrac{1}{\lambda_{\mathrm{p2}}} \pm \sqrt{\left(\dfrac{1}{\lambda_{\mathrm{p1}}}-\dfrac{1}{\lambda_{\mathrm{p2}}}\right)^2-\dfrac{4\mu(2r+1)}{m}}}. \end{cases} \tag{23}$$

For the subsequent analysis, the 3-dB bandwidth of the signal gain is of primary interest. Through lucubrating, it is found that the 3-dB bandwidth is mainly determined by the contribution of the non-degenerate FWM effect, so we pay more attention to Eq. (17). The 3-dB bandwidth can be obtained by setting

$$\frac{1+\left[\dfrac{\mu r}{g_{12}}\sinh(g_{12}L)\right]^2}{1+(\mu rL)^2} = \frac{1}{2}. \tag{24}$$

By simplification, Eq. (24) can be written as

$$\frac{(\mu rL)^2-1}{2(\mu rL)^2} = \left[\frac{\sinh(g_{12}L)}{g_{12}L}\right]^2. \tag{25}$$

The implications of the parameters μ, r, and g_{12} are the same as Eq. (18), and the parameters μ and r are related to pumping powers P_{p1} and P_{p2}, whereas g_{12} is dependent on P_{p1}, P_{p2}, λ_{p1} and λ_{p2}. From Eq. (25), we can get the solutions λ_{s1} and λ_{s2} by Newton downhill (ND) method, and the 3-dB bandwidth is defined as $\Delta\lambda = |\lambda_{\mathrm{s1}}-\lambda_{\mathrm{s2}}|$. In order to reveal the factors influencing the 3-dB bandwidth characteristic, we can discuss it from the following two aspects. Firstly, fixing P_{p1} and P_{p2}, the left-hand side of Eq. (25) is constant, and let λ_{p1} and λ_{p2} vary, a curve for $\Delta\lambda$ versus λ_{p1} and λ_{p2} can be obtained. Secondly, fixing λ_{p1} and λ_{p2}, let P_{p1} and P_{p2} vary, the relation between $\Delta\lambda$ and P_{p1} (or P_{p2}) is available. To analyze Eq. (25), in the real number region, the fact that $\dfrac{(\mu rL)^2-1}{2(\mu rL)^2} < \dfrac{1}{2}$ and $\left(\dfrac{\sinh(g_{12}L)}{g_{12}L}\right)^2 > 1$ exists, so there is no real root satisfying Eq. (25). But in the imaginary number region, we can yield imaginary roots by the ND method. Supposing $g_{12} = \mathrm{i}g_0$, and substituting it into Eq. (25), it can be written in another form as

$$\frac{(\mu rL)^2-1}{2(\mu rL)^2} = \left[\frac{\sin(g_0L)}{g_0L}\right]^2 = [\mathrm{sinc}(g_0L)]^2. \tag{26}$$

From Eq. (26), it is found that the left-hand side of it is constant if we fix the pumping powers, and g_0 is concerned on P_{p1} and P_{p2}. To solve Eq. (26), we can get the 3-dB bandwidth given by

$$\Delta\lambda = \frac{\sqrt{\left(\dfrac{1}{\lambda_{\mathrm{p1}}}-\dfrac{1}{\lambda_{\mathrm{p2}}}\right)^2+4M}}{\dfrac{1}{\lambda_{\mathrm{p1}}\lambda_{\mathrm{p2}}}-M}, \tag{27}$$

where

$$M = \frac{-u \pm 2\sqrt{(ur)^2+g_0^2}}{\pi\lambda_0^3 c\dfrac{\mathrm{d}D}{\mathrm{d}\lambda}\left[\lambda_0\left(\dfrac{1}{\lambda_{\mathrm{p1}}}+\dfrac{1}{\lambda_{\mathrm{p2}}}\right)-2\right]}. \tag{28}$$

Remarkably, it can be found that when $\frac{1}{\lambda_{p1}\lambda_{p2}} = M$, the 3-dB bandwidth will be approximately approaching infinity.

4 Numerical simulations and results

In the numerical calculations, the pump-1 and pump-2 powers are both 1 W, and the signal power is 0.1 mW. A typical HNLF with a length of 30 m and a zero dispersion slope of 0.031 ps/(nm^2·km) is used in our calculations. The nonlinear coefficient is 20 $(\mathrm{km\cdot W})^{-1}$, the dispersion zero wavelength is 1550 nm, and c is the light velocity in the vacuum.

Figure 3 illustrates the plot of calculated signal gain for a degenerate FOPA configuration with $\lambda_{p1} = 1540$ nm, as shown in the solid line. From the figure, we can know that the signal gain curve is centrosymmetric in some extent, and the filled dots in the dashed line represent the signal wavelengths satisfying the equation $\sinh(gL)/(gL) = 0$, which also determines the distribution of the side lobe valley points in the signal gain; the corresponding relations are shown in the figure marked by the arrow line. Therefore, a qualitative conclusion can be drawn that the signal gain structure is essentially determined by the equation $\sinh(gL)/(gL) = 0$ in some extent.

Figure 4 shows the plot of the calculated signal gain for a non-degenerate FOPA configuration with $\lambda_{p1} = 1540$ nm, $\lambda_{p2} = 1560$ nm. Note that we present the signal gain with the case of only the non-degenerated FWM occurring and neglect the degenerated FWM effect acting on the signal. From the dashed line in Fig. 4, it can be found that the plot of the function $y = \sinh(gL)/(gL)$ is not centrosymmetric, leading to the non-centrosymmetrical configuration of the signal gain. The solutions of $\sinh(gL)/(gL) = 0$ are also corresponding to the side lobe valley points of the signal gain shown by the dots in the dashed line in Fig. 4, and the corresponding relations are shown in the figure marked by the arrow line. The physical mechanism of this non-centrosymmetrical structure originates from the different injected pump wavelengths.

In the actual dual-pumped FOPA model, the degenerate and non-degenerate FWM effects compete with each other to amplify signal. Neglecting the pumping power depletion, the signal gain is shown in Fig. 5(d), which presents the calculated signal gain at $\lambda_{p1} = 1540$ nm, $\lambda_{p2} = 1560$ nm for a dual-pumped FOPA when considering degenerate FWM acting on the signal. Figure 5(a) shows the signal gain when each pump acts on the signal, respectively. Because of the severe phase mismatching, signal gain is not very high with its maximum value approximately 1.6 dB. Figure 5(b) represents the superposition of the two degenerate OPA signal gains. Figure 5(c) presents the calculated signal gain at $\lambda_{p1} = 1540$ nm, $\lambda_{p2} = 1560$ nm for a non-degenerate FOPA without considering degenerate FWM. The 3-dB bandwidth can be attained at 455.5 nm if the wavelengths and powers of the pump waves are properly chosen. Figure 5(d) shows the calculated signal gain in realistic circumstance at $\lambda_{p1} = 1540$ nm, $\lambda_{p2} = 1560$ nm for a non-degenerate FOPA when considering degenerate FWM. The small peak in the plot is owed to degenerate FWM contribution to the signal gain, and this confirms that the actual signal gain emanates from both the degenerate and non-degenerate parametric processes in dual-pumped FOPA configuration, which is different from the reported literatures [1].

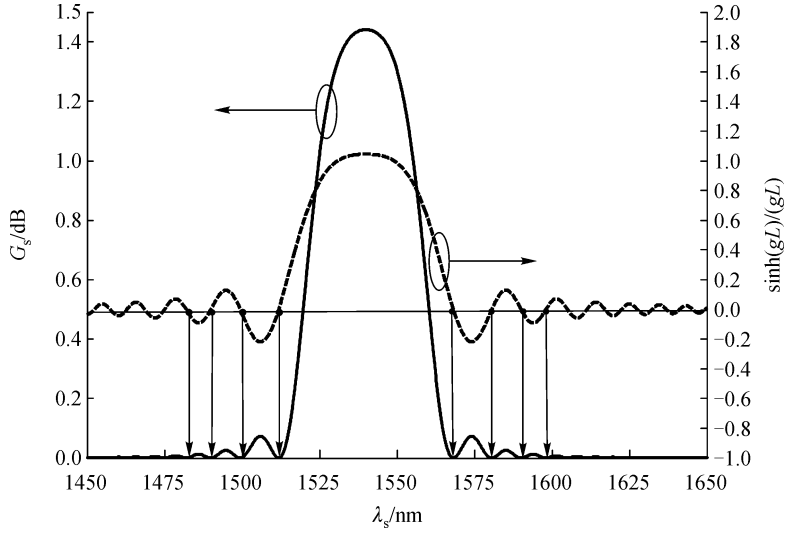


Fig. 3 Calculated signal gain for a degenerate FOPA with $\lambda_{p1} = 1540$ nm (solid line) and the relation for $\sinh(gL)/(gL)$ vs λ_s (dashed line) (parameters for FOPA are $P_1 = P_2 = 1$ W, $P_s = 0.1$ mW, $\lambda_0 = 1550$ nm, $\gamma = 20$ $(\mathrm{km\cdot W})^{-1}$, $\frac{\mathrm{d}D}{\mathrm{d}\lambda} = 0.031$ ps/(nm^2·km))

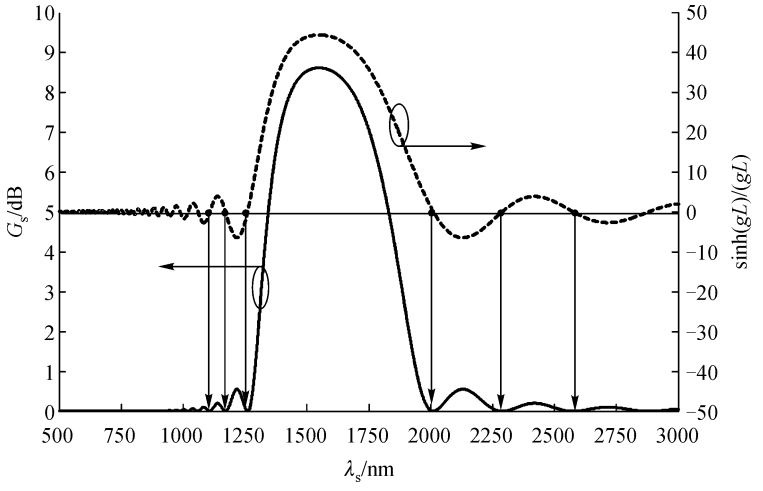


Fig. 4 Calculated signal gain at $\lambda_{p1} = 1540$ nm, $\lambda_{p2} = 1560$ nm for a non-degenerate FOPA without considering degenerate FWM acting on the signal (solid line) and the relation for $\sinh(gL)/(gL)$ vs λ_s (dashed line) (parameters for FOPA are $P_1 = P_2 = 1$ W, $P_s = 0.1$ mW, $\frac{dD}{d\lambda} = 0.031$ ps/(nm^2·km), $\lambda_0 = 1550$ nm, $\gamma = 20$ (km·W)$^{-1}$)

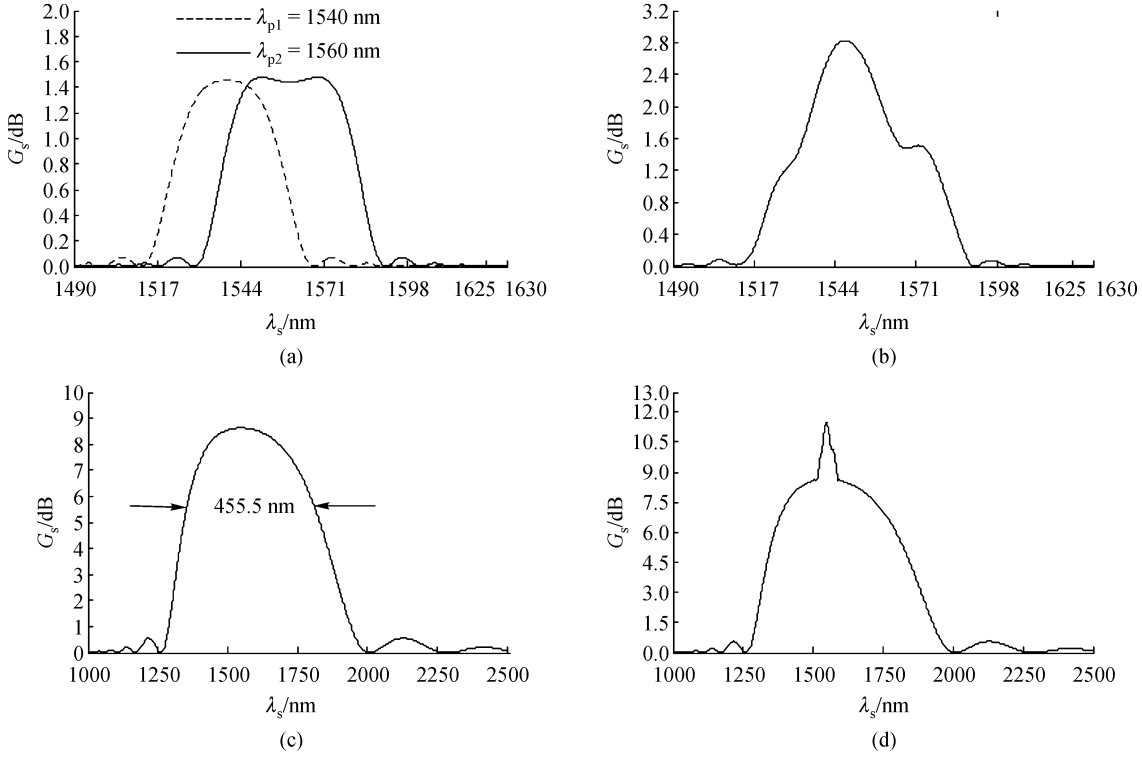


Fig. 5 Calculated signal gain at $\lambda_{p1} = 1540$ nm, $\lambda_{p2} = 1560$ nm for FOPA. (a) Signal gain of degenerate OPA at $\lambda_{p1} = 1540$ nm and $\lambda_{p2} = 1560$ nm, respectively; (b) combination of curves of (a); (c) signal gain of pure non-degenerate OPA; (d) actual signal gain of dual-pumped FOPA

Figure 6(a) presents the signal gain when each pump ($\lambda_{p1} = 1549$ nm, $\lambda_{p2} = 1552$ nm) amplifies the signal, respectively. As the pumping wavelengths are closed, the centre point of the signal gain approximately overlaps. A flat property of the superposition of two degenerate OPA signal gains is demonstrated in Fig. 6(b) owing to small detuning of the injected pump wavelengths. Similar with Fig. 5(c), Fig. 6(c) presents the calculated signal gain at $\lambda_{p1} = 1549$ nm and $\lambda_{p2} = 1552$ nm for a non-degenerate FOPA without considering degenerate FWM acting on the

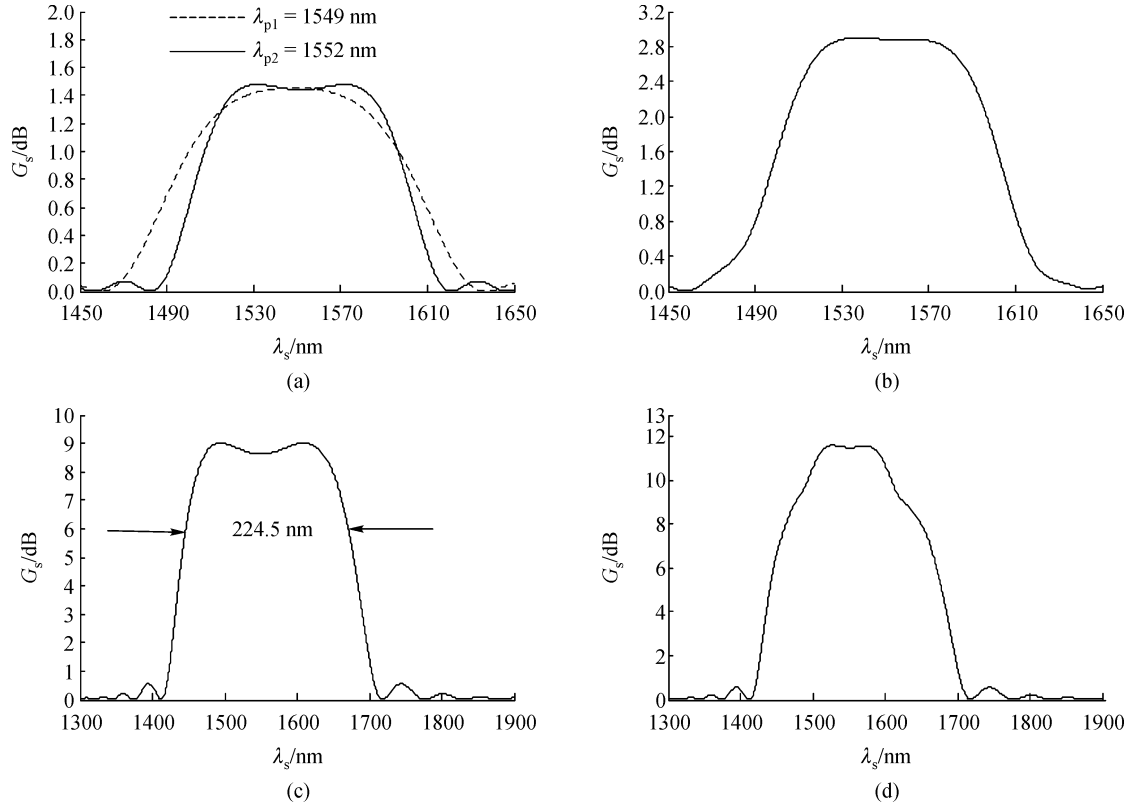


Fig. 6 Calculated signal gain at $\lambda_{p1} = 1549$ nm, $\lambda_{p2} = 1552$ nm for FOPA configuration. (a) Signal gain of degenerate OPA at $\lambda_{p1} =$ 1549 nm and $\lambda_{p2} = 1552$ nm, respectively; (b) combination of curves of (a); (c) signal gain of pure non-degenerate OPA; (d) actual signal gain of dual-pumped FOPA configuration

signal. Compared to Fig. 5(c), the 3-dB bandwidth decreases from 455.5 to 224.5 nm. Figure 6(d) shows an actually calculated gain for a non-degenerate FOPA when considering degenerate FWM acting on the signal. Different from Fig. 6(c), the center region of Fig. 6(d) subtly heaves because of the degenerate FWM effect contributing to it.

The implications of Figs. 7(a) and 7(b) are the same as those of Figs. 6(a) and 6(b), as discussed above. Figure 7(c) presents the signal gain for the non-degenerate FOPA. What interests us most is that when the pump wavelengths are tuned at $\lambda_{p1} = 1549$ nm and $\lambda_{p2} = 1551.02$ nm, the 3-dB bandwidth is sharply increased to 2253.4 nm, which has not been reported before in the literature. As the condition of $\frac{1}{\lambda_{p1}\lambda_{p2}} = M$ is approximately satisfied, the signal gain will be flat when the signal wavelength operates in a large range. The small peak emerging in Fig. 7(d) is also due to degenerate FWM effect acting on the signal as mentioned before.

A deep rooted investigation into the bandwidth of the signal gain is demonstrated in Fig. 8, and the implication of Fig. 8 is the same as that of Fig. 7. Differently, when setting $\lambda_{p1} = 1549$ nm and $\lambda_{p2} = 1551$ nm, there is an interesting phenomenon emerging that the 3-dB bandwidth of the signal gain is approximately infinite. The reason is that when the condition of $\frac{1}{\lambda_{p1}\lambda_{p2}} = M$ is strictly satisfied, the signal gain will be flat in an infinite signal wavelength range owing to Eq. (27).

Figure 9 depicts the calculated 3-dB bandwidth versus λ_{p1} when $\lambda_{p2} = 1547, 1549, 1550, 1551, 1553$ nm, respectively, from which we can clearly see that the center points of the calculated 3-dB bandwidth curves will emerge in the symmetrical position referred to the zero dispersion wavelength point. It is an interesting phenomenon that when $\lambda_{p1} = \lambda_{p2} = 1550$ nm, there is a sunken valley at the zero dispersion point. This can be easily explained from Eq. (27). When $\lambda_{p1} = \lambda_{p2} = \lambda_0 = 1550$ nm, $M = \infty$, and then $\Delta\lambda = 0$ nm, so there is a sunken valley in the plot.

Figure 10 shows the three-dimensional (3D) plot of the 3-dB bandwidth as a function of pumping wavelengths λ_{p1} and λ_{p2} with pumping powers tuned at $P_1 = 1$ W, $P_2 = 1$ W. From Fig. 10, it is found that the large 3-dB bandwidth region is distributed on the line of $\lambda_{p2} = -\lambda_{p1} + 3100$, and the maximum 3-dB bandwidth can be achieved at

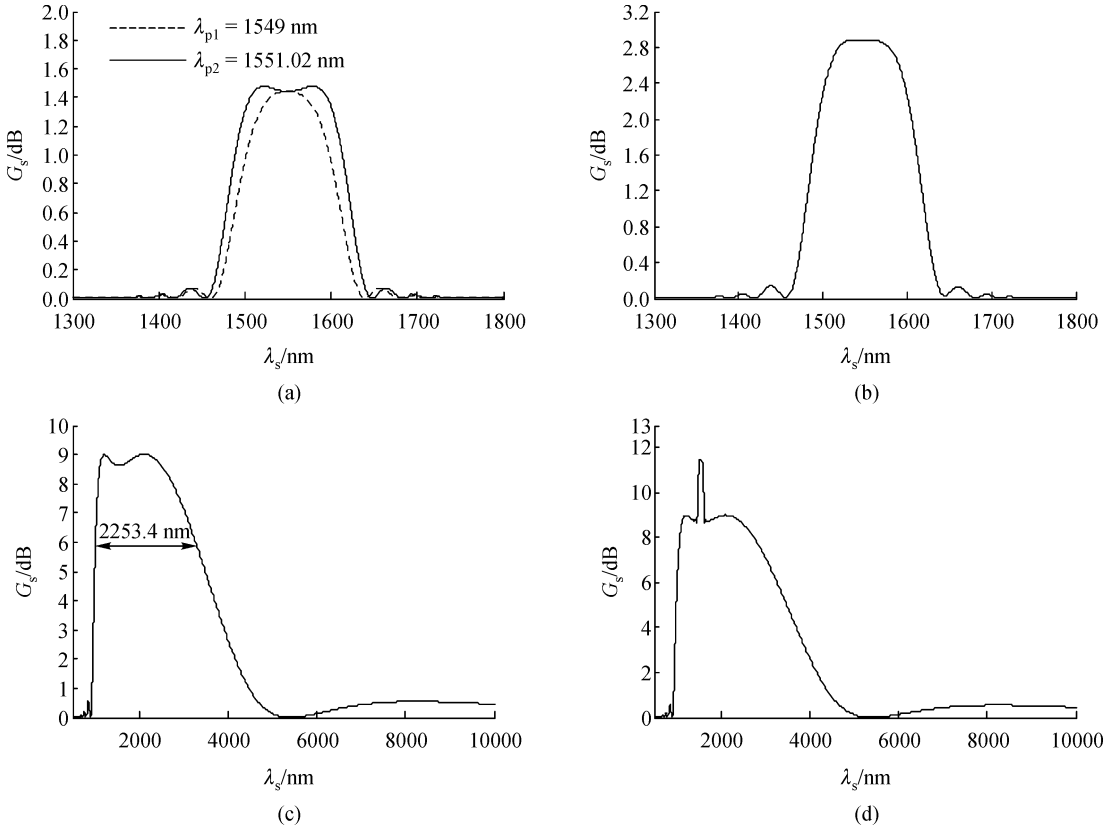


Fig. 7 Calculated gain at $\lambda_{p1} = 1549$ nm, $\lambda_{p2} = 1551.02$ nm for FOPA. (a) Signal gain of degenerate OPA at $\lambda_{p1} = 1549$ nm and $\lambda_{p2} = 1551.02$ nm, respectively; (b) combination of curves of (a); (c) signal gain of pure non-degenerate OPA; (d) actual signal gain of dual-pumped FOPA

10000 nm, as shown in the color region. The blue region represents the low 3-dB bandwidth fluctuated approximately from 0 to 200 nm.

Moreover, we report the calculated 3-dB bandwidth as a function of P_1 when setting the wavelengths at (1547, 1549), (1547, 1551), (1551, 1553), (1551, 1555), respectively, as shown in Figs. 11(a), 11(b), 11(c) and 11(d). From Figs. 11(a) and 11(b), we can see that the 3-dB bandwidth will be monotonously decreased with the increasing of P_1 when setting the P_2 at 0.6, 0.8, 1, 1.2 W, respectively, and it is different from Figs. 11(c) and 11(d), which is decreased with increasing of P_1 firstly, and then increased with P_2. It is worth noting that the 3-dB bandwidth is not very high, ranging from about 90 to 160 nm.

Figure 12 shows the calculated 3-dB bandwidth as a function of input pumping power P_2, from which we can see that the 3-dB bandwidth will fluctuate from 2000 to 10000 nm when P_1 is set around 0.5 W. This confirms that large $\Delta\lambda$ can be obtained by just choosing the pumping wavelengths and powers. When $\lambda_{p1} = 1547$ nm, $\lambda_{p2} = 1549$ nm, $\Delta\lambda$ will sharply decrease in some extent to around 250 nm when P_2 tuned at about 0.557 W, as shown in the blue line. However, when $\lambda_{p1} = 1551$ nm, $\lambda_{p2} = 1555$ nm, $\Delta\lambda$ will sharply decrease to around 200 nm when P_2 tuned just at about 0.539 W, as shown in the red line. This phenomenon will be further pointed out at the following simulations.

Figure 13 displays the 3D plot of the 3-dB bandwidth as a function of P_1 and P_2 at the wavelengths $\lambda_{p1} = 1547$ nm and $\lambda_{p2} = 1549$ nm. It is worth noting that when P_1 and P_2 both range from about 0.4 to 0.5 W, the maximum 3-dB bandwidth will be maximum achieved at 10000 nm, as shown in the color region in Fig. 13(a). When seeing the plot of Fig. 13(a) from the angle of the P_2 axis, it is consistent with the blue line of Fig. 12 at $P_2 = 0.5$ W point. Figure 13(b) corresponds with the Fig. 13(a) blue region, which shows that the 3-dB bandwidth will be monotonously decreased with the increasing of P_1 and P_2 simultaneously, and when P_1 and P_2 range from 0.5 to 1.5 W, the 3-dB bandwidth fluctuates from 70 to 95 nm.

Figure 14 illustrates the 3D plot of the 3-dB bandwidth as a function of P_1 and P_2 at the wavelengths $\lambda_{p1} = 1551$ nm and $\lambda_{p2} = 1555$ nm. Figure 14(a) is almost the same with Fig. 13(a), and it is also found that when seeing Fig. 14(a) from the angle of the P_2 axis, it is consistent with the red line of Fig. 12 at $P_2 = 0.5$ W point. However, there is a subtle difference between Figs. 13(b) and 14(b). From

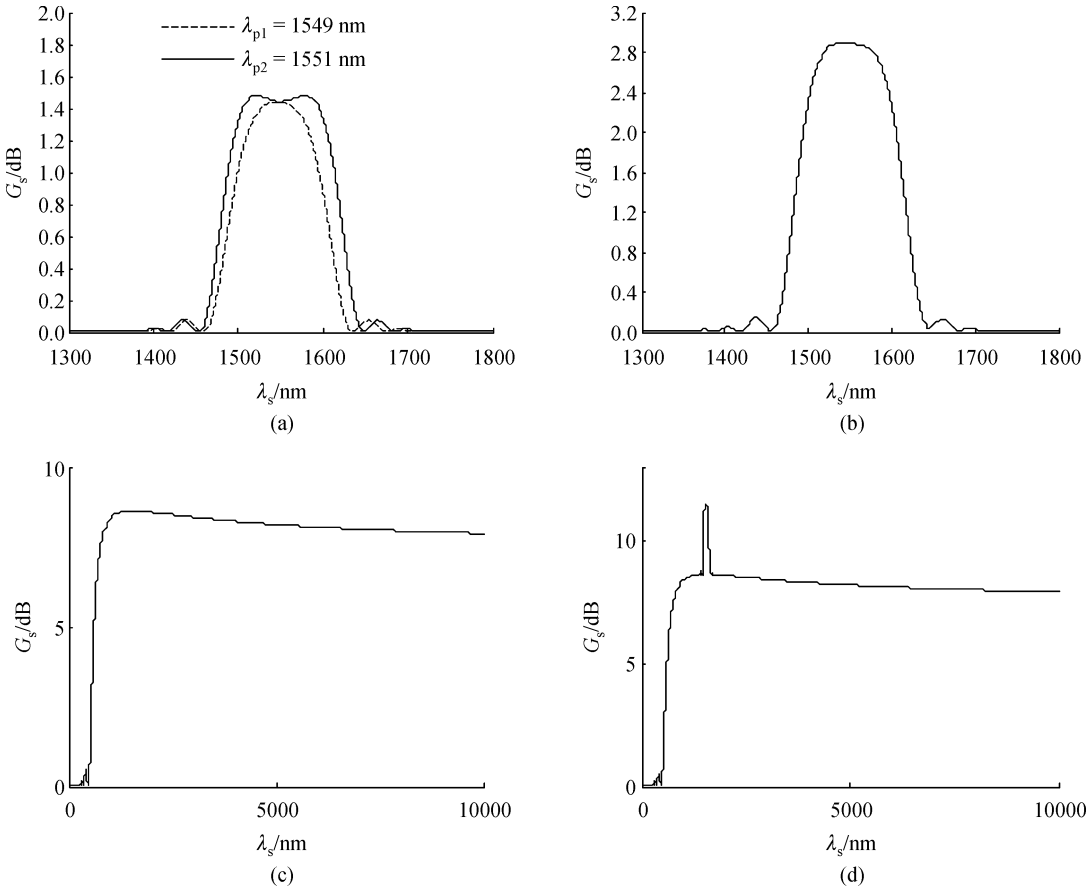


Fig. 8 Calculated signal gain with pump wavelengths $\lambda_{p1} = 1549$ nm, $\lambda_{p2} = 1551$ nm for FOPA. (a) Signal gain of degenerate OPA configuration with $\lambda_{p1} = 1549$ nm and $\lambda_{p2} = 1551$ nm, respectively; (b) combination of curves of (a); (c) signal gain of pure non-degenerate OPA; (d) actual signal gain of dual-pumped FOPA configuration

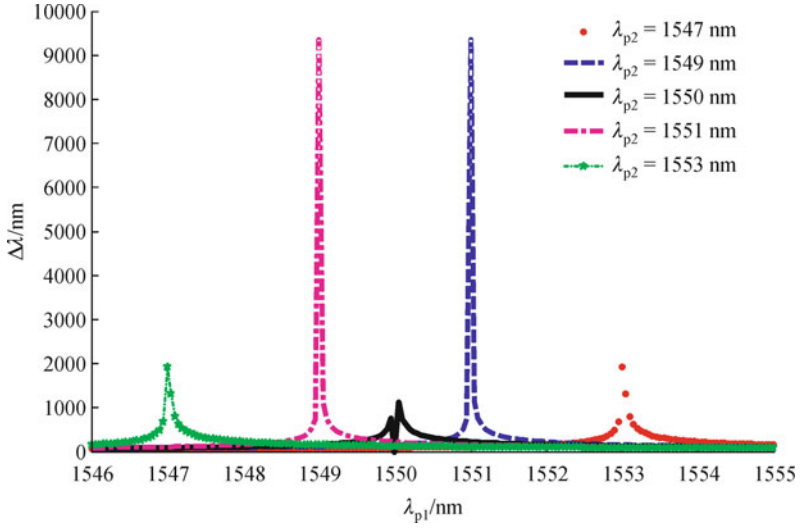


Fig. 9 Calculated 3-dB bandwidth versus λ_{p1} when setting $\lambda_{p2} = 1547, 1549, 1550, 1551, 1553$ nm marked with different color respectively

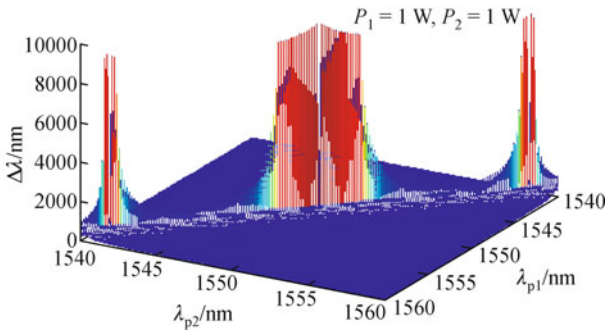


Fig. 10 Calculated 3-dB bandwidth as a function of pumping wavelengths λ_{p1} and λ_{p2} with pumping powers tuned at $P_1 = 1$ W, $P_2 = 1$ W

Fig. 14(b), it is shown that when P_1 and P_2 range from 0.5 to 0.8 W, the 3-dB bandwidth is decreased with the increasing of P_1 and P_2 simultaneously. But when P_1 and P_2 range from 0.8 to 1.5 W, the 3-dB bandwidth is increased with P_1 and P_2 simultaneously, which corresponds to Fig. 11(d).

Figure 15 shows calculated pumping wavelength relations satisfying the condition of the 3-dB bandwidth $\Delta\lambda = 500$ nm with $P_1 = 1$ W, $P_2 = 1$ W. It can be found that when λ_{p1} ranges from 1000 to 2000 nm, λ_{p2} is almost linearly increased with λ_{p1} except in the range of 1300–1360 nm and 1820–1900 nm. Additionally, the plot is symmetrical from the line of $\lambda_{p2} = \lambda_{p1}$. This can be well interpreted by Eq. (27). When $\Delta\lambda$ is constant, exchanging the position of λ_{p1} and λ_{p2}, the essence of Eq. (27) is not varied, so the curves of Fig. 15 are symmetrical on the line of $\lambda_{p2} = \lambda_{p1}$. When λ_{p1} ranges from 1300 to 1360 nm and from 1820 to 1900 nm, Eq. (27) presents the property of ellipse, and thus, there are numbers of ellipse emerging in the plot. While λ_{p1} ranges in the other region, Eq. (27) presents the linear characteristic, so λ_{p2} is linearly increased with λ_{p1}.

Figure 16 shows calculated pumping wavelength relations satisfying the conditions of the 3-dB bandwidth $\Delta\lambda = 400, 600, 800$ nm, respectively, with $P_1 = 0.5$ W, $P_2 = 1$ W. From Fig. 16, it can be easily found that the curves are symmetrical on the line of $\lambda_{p2} = \lambda_{p1}$, and when increasing $\Delta\lambda$, the curve is far away from the line of $\lambda_{p2} = \lambda_{p1}$, which implies that the 3-dB bandwidth can be governed by properly choosing the injected wavelengths. Remarkably, the red, black and blue lines represent the injected wavelength relations with the 3-dB bandwidth $\Delta\lambda = 400, 600$ and 800 nm, respectively.

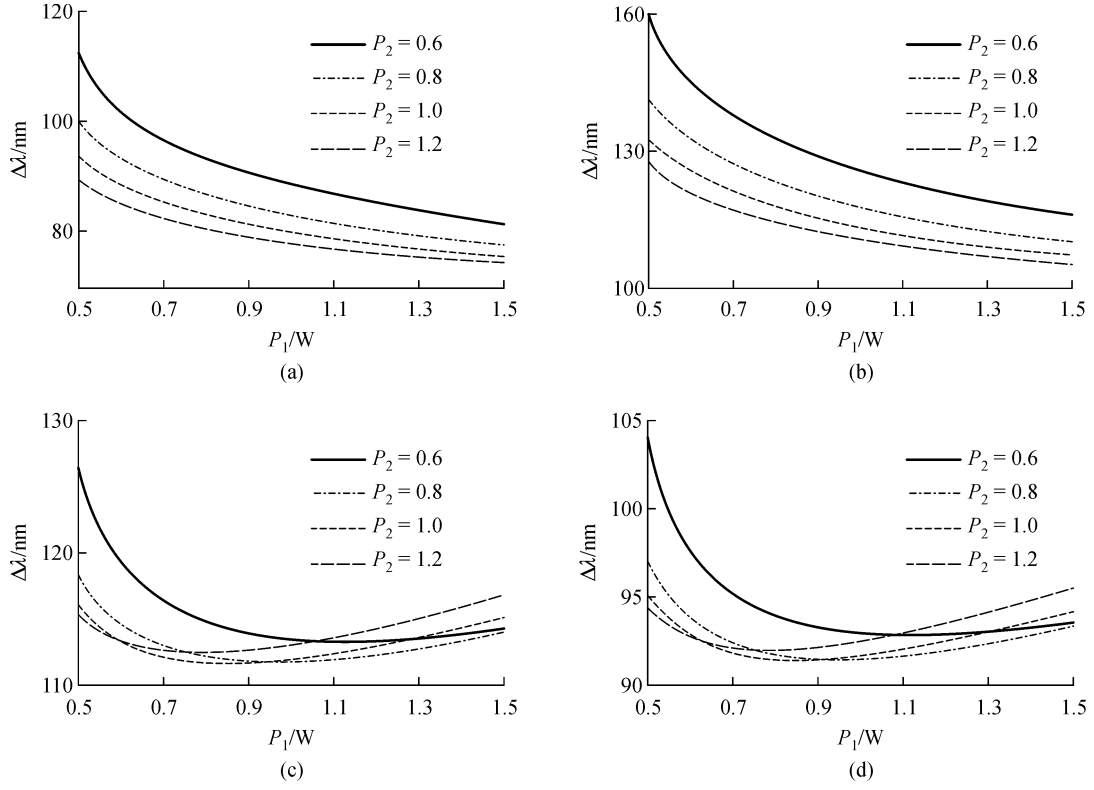


Fig. 11 Calculated 3-dB bandwidth versus P_1 when setting different pumping wavelengths and different P_2. (a) $\lambda_{p1} = 1547$ nm and $\lambda_{p2} = 1549$ nm; (b) $\lambda_{p1} = 1547$ nm and $\lambda_{p2} = 1551$ nm; (c) $\lambda_{p1} = 1551$ nm and $\lambda_{p2} = 1553$ nm; (d) $\lambda_{p1} = 1551$ nm and $\lambda_{p2} = 1555$ nm

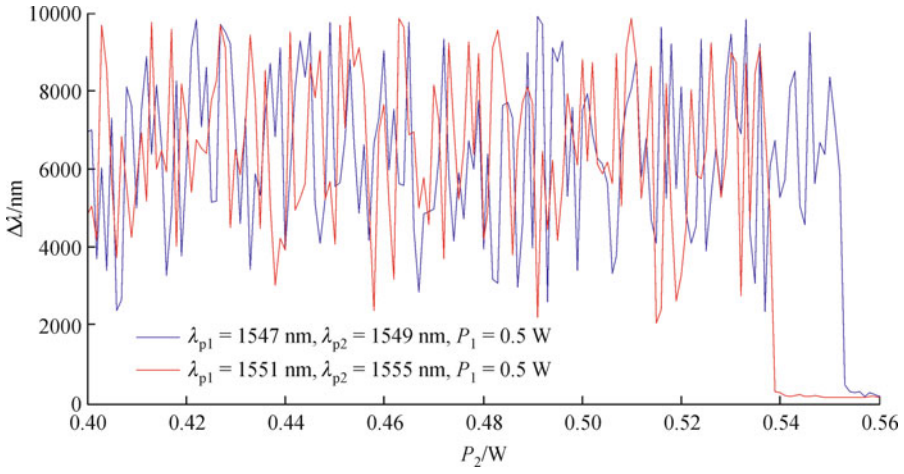


Fig. 12 Calculated 3-dB bandwidth as a function of input pumping power P_2 with P_1 setting at 0.5 W (blue line represents $\Delta\lambda$ versus P_2 with $\lambda_{p1} = 1547$ nm, $\lambda_{p2} = 1549$ nm, and red line shows $\Delta\lambda$ versus P_2 with $\lambda_{p1} = 1551$ nm, $\lambda_{p2} = 1555$ nm)

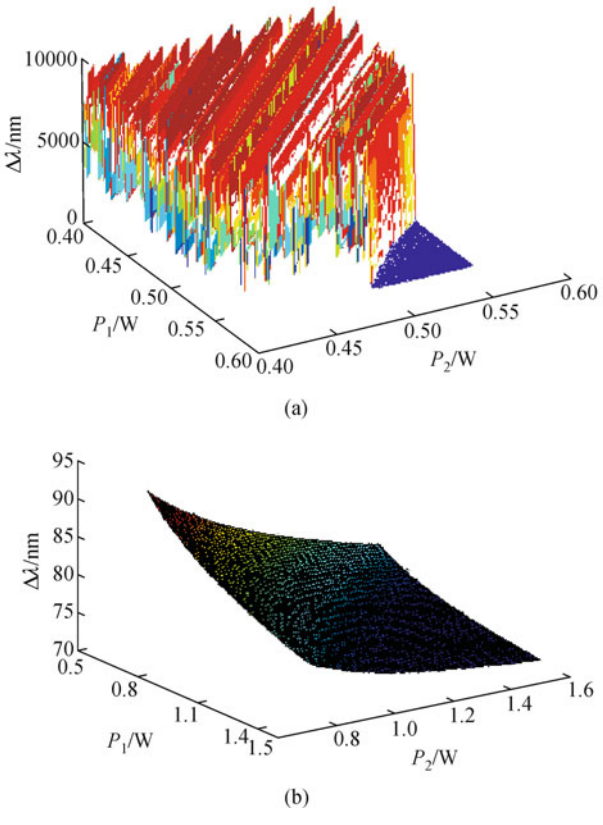


Fig. 13 3D plot for calculated 3-dB bandwidth as a function of input pumping power P_1 and P_2 with pumping wavelengths tuned at $\lambda_{p1} = 1547$ nm and $\lambda_{p2} = 1549$ nm. (a) P_1 and P_2 both range from 0.4 to 0.55 W; (b) P_1 and P_2 both range from 0.55 to 1.5 W

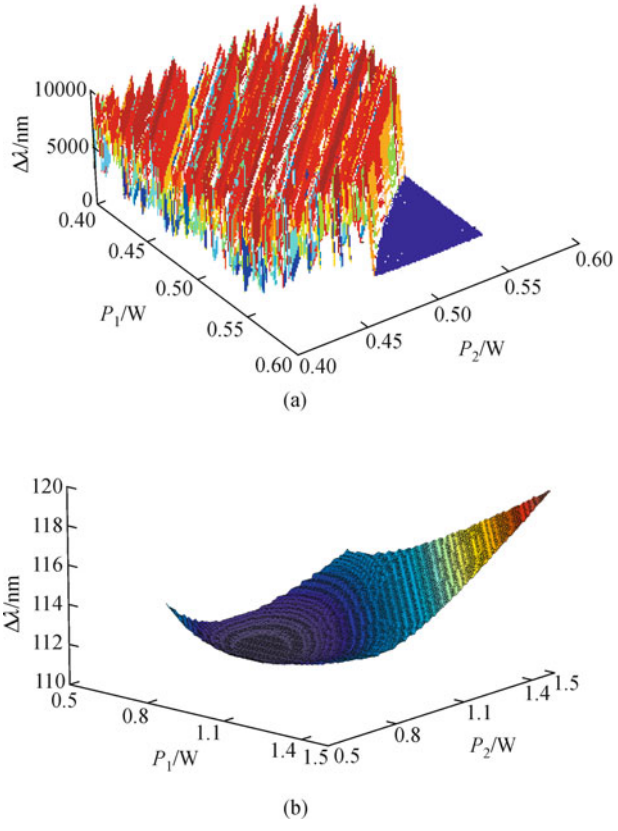


Fig. 14 3D plot for calculated 3-dB bandwidth as a function of input pumping power P_1 and P_2 with pumping wavelengths tuned at $\lambda_{p1} = 1551$ nm, $\lambda_{p2} = 1555$ nm (parameters for FOPA are $\frac{dD}{d\lambda} = 0.031$ ps/(nm^2·km), $\lambda_0 = 1550$ nm, $\gamma = 20$ (km·W)$^{-1}$). (a) P_1 and P_2 both range from 0.4 to 0.55 W; (b) P_1 and P_2 both range from 0.55 to 1.5 W

5 Conclusions

We theoretically proposed a mode for dual-pumped FOPA configuration under the un-depletion mode. The assumption that degenerate and non-degenerate FWMs occur in sequence is firstly demonstrated, based on which

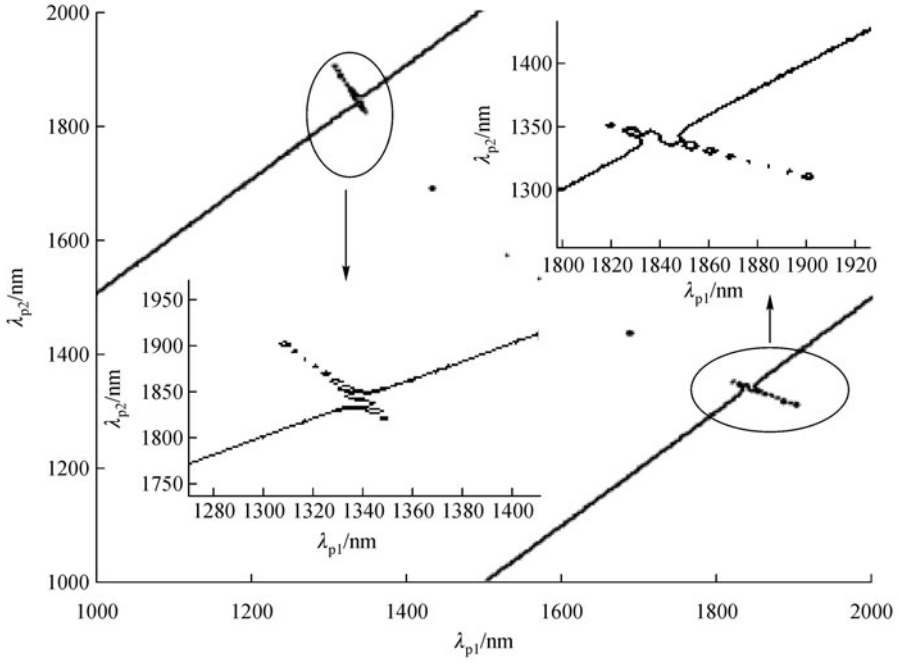


Fig. 15 Calculated pumping wavelengths relations satisfying condition of 3-dB bandwidth $\Delta\lambda = 500$ nm with $P_1 = 1$ W, $P_2 = 1$ W (other parameters for FOPA are $\frac{dD}{d\lambda} = 0.031$ ps/(nm^2·km), $\lambda_0 = 1550$ nm, $\gamma = 20$ (km·W)$^{-1}$)

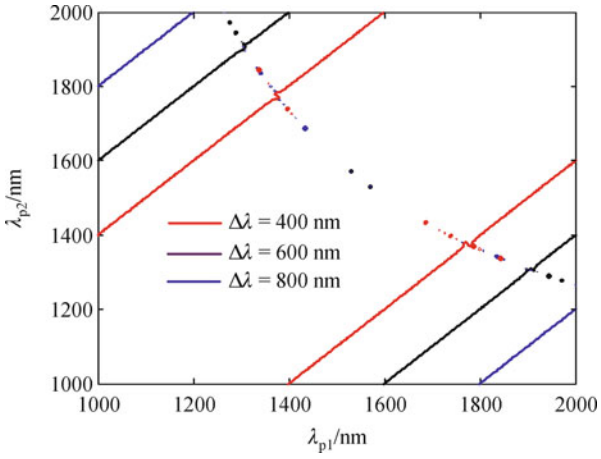


Fig. 16 Calculated pumping wavelengths relations satisfying conditions of 3-dB bandwidth $\Delta\lambda = 400, 600, 800$ nm, respectively with $P_1 = 0.5$ W and $P_2 = 1$ W (parameters for FOPA are $\frac{dD}{d\lambda} = 0.031$ ps/(nm^2·km), $\lambda_0 = 1550$ nm, $\gamma = 20$ (km·W)$^{-1}$)

the analytical expressions for the signal gain and the 3-dB bandwidth are thus yielded. Simulations show that the realistic signal gain spectrum in our model is composed of three sections, and there is a pinnacle emerging because of the contribution of the degenerate parametric process. The 3-dB bandwidth of the signal gain is mainly determined by the performance of non-degenerate FWM, which can be attained about 2253.4 nm theoretically by properly setting the pumping powers. These may find great potential applications in future high-speed all-optical signal processing, such as all-optical wavelength conversion, optical amplifier, and all-optical sampling.

References

1. Hansryd J, Andrekson P A, Westlund M, Li J, Hedekvist P O. Fiber-based optical parametric amplifiers and their applications. IEEE Journal on Selected Topics in Quantum Electronics, 2002, 8(3): 506–520
2. Sun J Q, Li H, Cheng Y, Li J. Tunable wavelength conversion of picosecond pulses based on cascaded sum- and difference-frequency generation in quasi-phase-matched $LiNbO_3$ waveguides. Optics Communications, 2008, 281(23): 5874–5883
3. Jargon J A, Wu X, Choi H Y, Chung Y C, Willner A E. Optical performance monitoring of QPSK data channels by use of neural networks trained with parameters derived from asynchronous constellation diagrams. Optics Express, 2010, 18(5): 4931–4938
4. Van Erps J, Luan F, Pelusi M D, Iredale T, Madden S, Choi D Y, Bulla D A, Luther-Davies B, Thienpont H, Eggleton B J. High-resolution optical sampling of 640-Gb/s data using four-wave mixing in dispersion-engineered highly nonlinear As_2S_3 planar waveguides. Journal of Lightwave Technology, 2010, 28(2): 209–215
5. Torounidis T, Karlsson M, Andrekson P A. Fiber optical parametric amplifier pulse source: theory and experiments. Journal of Lightwave Technology, 2005, 23(12): 4067–4073

6. Zhao L, Sun J Q. Investigation of tunable trap filter utilizing intense signal four wave mixing model in highly non-linear fiber. Optics Communications, 2009, 282(14): 2975–2982
7. Gao M Y, Jiang C, Hu W S. Dual-pump broadband fiber optical parametric amplifier with a three-section photonic crystal fiber scheme. Proceedings of SPIE, 2005, 5623: 300–307
8. Liu X M, Zhou X Q, Lu C. Multiple four-wave mixing self-stability in optical fibers. Physical Review A, 2005, 72(1): 013811
9. Liu X M. Theory and experiments for multiple four-wave-mixing processes with multifrequency pumps in optical fibers. Physical Review A, 2008, 77(4): 043818
10. Zhao L, Sun J Q. Suppression of degenerate four-wave mixing in nondegenerate optical parametric amplifiers. Optical Engineering, 2008, 47(8): 085001
11. Cao H, Sun J Q, Huang D X. Unique dispersion effects on transmitting and amplifying of picosecond pulses in fiber optical parametric amplifiers. Proceedings of SPIE, 2005, 6019: 601931
12. Cao H, Sun J Q, Huang D X. Theoretical study on the signal pulse splitting phenomenon in continuous wave pumped fiber optical parametric amplifier. Proceedings of SPIE, 2005, 6019: 601930